NeuroImage 183 (2018) 544–552

Contents lists available at ScienceDirect

NeuroImage

journal homepage: www.elsevier.com/locate/neuroimage

Voxel-wise detection of functional networks in white matter

Yali Huang [a,b], Stephen K. Bailey [c], Peiguang Wang [b], Laurie E. Cutting [c,d,e], John C. Gore [a,c,d,f,g], Zhaohua Ding [a,g,h,*]

[a] Vanderbilt University Institute of Imaging Science, Nashville, TN, 37232, United States
[b] College of Electronics and Information Engineering, Hebei University, Baoding, 071002, PR China
[c] Vanderbilt Brain Institute, Vanderbilt University, Nashville, TN, 37232, United States
[d] Vanderbilt Kennedy Center, Vanderbilt University, Nashville, TN, 37232, United States
[e] Peabody College of Education and Human Development, Vanderbilt University, Nashville, TN, 37232, United States
[f] Department of Radiology and Radiological Sciences, Vanderbilt University Medical Center, Nashville, TN, 37232, United States
[g] Department of Biomedical Engineering, Vanderbilt University, Nashville, TN, 37232, United States
[h] Department of Electrical Engineering and Computer Science, Vanderbilt University, Nashville, TN, 37232, United States

ARTICLE INFO

Keywords:
fMRI
BOLD
White matter
Functional activation
Visual stimulation

ABSTRACT

Functional magnetic resonance imaging (fMRI) depicts neural activity in the brain indirectly by measuring blood oxygenation level dependent (BOLD) signals. The majority of fMRI studies have focused on detecting cortical activity in gray matter (GM), but whether functional BOLD signal changes also arise in white matter (WM), and whether neural activities trigger hemodynamic changes in WM similarly to GM, remain controversial, particularly in light of the much lower vascular density in WM. However, BOLD effects in WM are readily detected under hypercapnic challenges, and the number of reports supporting reliable detections of stimulus-induced activations in WM continues to grow. Rather than assume a particular hemodynamic response function, we used a voxel-by-voxel analysis of frequency spectra in WM to detect WM activations under visual stimulation, whose locations were validated with fiber tractography using diffusion tensor imaging (DTI). We demonstrate that specific WM regions are robustly activated in response to visual stimulation, and that regional distributions of WM activation are consistent with fiber pathways reconstructed using DTI. We further examined the variation in the concordance between WM activation and fiber density in groups of different sample sizes, and compared the signal profiles of BOLD time series between resting state and visual stimulation conditions in activated GM as well as activated and non-activated WM regions. Our findings confirm that BOLD signal variations in WM are modulated by neural activity and are detectable with conventional fMRI using appropriate methods, thus offering the potential of expanding functional connectivity measurements throughout the brain.

1. Introduction

Functional MRI (fMRI) has been widely used to detect neural activities in the brain on the basis of changes in blood oxygenation level dependent (BOLD) signals (Ogawa et al., 1990; Biswal et al., 1995). Conventional functional images are usually acquired with subjects either responding to a stimulus or performing a task or in a resting state. When subject to a functional load, activated brain regions relevant to the function can be localized (Gore, 2003; Glover, 2011), whereas in a resting state, functional connections between brain regions may be inferred (Raichle et al., 2001; Buckner et al., 2008; Fox and Raichle, 2007). Despite their widespread applications as a research and clinical tool, fMRI studies have been almost exclusively focused on the detection of functional activity or connectivity in gray matter (GM), with only rare reports of BOLD effects in the connection pathways in white matter (WM) that convey neural signals among the GM regions.

In the published literature there have in fact been open debates as to whether neural activity actually elicits hemodynamic responses in WM similar to those measureable in GM (Logothetis and Wandell, 2004; Gawryluk et al., 2014). Physiologically, WM possesses much less dense vasculature than GM (Nonaka et al., 2003), and has lower blood flow, and so neural activity therein may be expected to trigger much smaller hemodynamic responses if they occur. However, regardless of the large discrepancies in vascular density between WM and GM, BOLD effects in

* Corresponding author. Vanderbilt University Institute of Imaging Science, Vanderbilt University Medical Center, R-1302 Medical Center North, Nashville, TN, 37232, United States.
E-mail address: zhaohua.ding@vanderbilt.edu (Z. Ding).

https://doi.org/10.1016/j.neuroimage.2018.08.049
Received 8 February 2018; Received in revised form 19 August 2018; Accepted 20 August 2018
Available online 23 August 2018

WM in response to hypercapnic challenges are almost half those of GM (Rostrup et al., 2000), WM contains a higher ratio of glial cells to neurons (Azevedo et al., 2009) that are metabolically active, and the oxygen extraction fractions in WM and GM have been measured to be approximately equal (Raichle et al., 2001). In addition, it has been observed that BOLD signals in both WM and GM exhibit similar temporal and spectral profiles in the resting brain (Ding et al., 2013), and their low frequency (0.01–0.08 Hz) fractional signal powers are largely comparable (Ding et al., 2016). Some studies have shown convincingly that transient external stimuli can reliably induce a hemodynamic response in WM with a profile similar to that in GM, but stretched in time and with smaller peak amplitude (Yarkoni et al., 2009; Fraser et al., 2012). Taken together, these findings converge to suggest that there are no fundamental barriers against the possibility of detecting neural activities in WM (Gawryluk et al., 2014), though more sensitive imaging or analysis methods may be required.

Recently a small but increasing number of reports have provided convincing evidence that changes in neural activity cause corresponding signal changes in WM that are measurable with conventional fMRI (Gawryluk et al., 2014). For example, it has been observed that such changes could be detected with special task paradigms (Yarkoni et al., 2009; Gawryluk et al., 2009). These reports of functional activations of WM were later confirmed by experiments with sensory stimulations and motor tasks that demonstrated BOLD responses in the corpus callosum (Fabri et al., 2011), and along parts of projection pathways (Wu et al., 2017). In particular, it was found that the detectability of BOLD signals in WM enhances with high field fMRI (Mazerolle et al., 2013) and specialized imaging sequences (Gawryluk et al., 2009) or when a specific hemodynamic response in WM is considered (Courtemanche et al., 2017).

In parallel with the detection of WM activations under functional loading, BOLD signals in a resting state have also been reported which appear to reflect neural activity in WM. For instance, Ding et al. observed that BOLD signals in WM exhibit structure-specific anisotropic correlations, that these coincide with fiber patterns revealed by diffusion tensor imaging (DTI), and that external stimuli alter the patterns and degrees of correlation in functionally relevant structures (Ding et al., 2013, 2016). Meanwhile, Marussich et al. found BOLD signals in WM are hierarchically organized into axonal fiber bundles, and are reorganized during steady-state natural vision (Marussich et al., 2017). More recently, Peer et al. identified intrinsic functional networks in WM, which correspond to structural networks defined independently by DTI, and further found signals in these functional networks are correlated with those in GM functional networks (Peer et al., 2017).

We have observed previously that resting state BOLD signals in certain WM tracts show significant correlations with specific GM regions, which can be modulated by functional loading, and that WM signal profiles exhibit clear specificity to the functional loading (Ding et al., 2018). The purpose of this work is to more comprehensively examine the robustness and sensitivity of detecting BOLD signals in WM using a voxel-wise analysis without assuming any specific hemodynamic response function. Briefly, we analyze BOLD signals voxel-wise in WM in both temporal and frequency domains under resting state and visual stimulation conditions. We then compare activation maps derived from signal frequency spectra with the corresponding visual pathways reconstructed by DTI-based tractography. We also evaluate the degree of concordance between WM activations and fiber density within a group for different sizes of the subject group which represents a metric of sensitivity for detecting WM activity. To examine how BOLD signals vary between tissues, we compare the temporal characteristics of BOLD signals between GM and WM, during both resting state and visual stimulation. Findings from this series of experiments strongly support that BOLD signal fluctuations in WM reflect intrinsic neural activity, and that these hemodynamic indicators of neural activity are reliably measurable with appropriate methods, thus suggesting a new avenue of neuroimaging research.

2. Materials and methods

2.1. Subjects and image acquisitions

The imaging data analyzed were part of the datasets we used in a previous study (Ding et al., 2018). We acquired functional imaging data from fourteen right handed, healthy volunteers (mean age: 28.8 ± 5.0 years; range: 23–37 years). No subjects had a history of neurological, psychiatric or medical conditions as determined by interview. The subject recruitment and image acquisition were carried out in accordance with protocols approved by the Institutional Review Board at Vanderbilt University.

Two fMRI acquisitions for each subject were selected for this study. In the first session, subjects were asked to rest in the scanner with their eyes closed; and in the second session, they were exposed to visual stimulation during which they viewed alternately a dark screen with crosshair and a flashing checkerboard (8 Hz) projected onto a screen mounted in the back of the scanner bore. The stimulations began with 15 s of crosshair, followed by alternating 30 s block of flashing checkerboard and crosshair, for a total of seven blocks for each condition. Note that for the stimulus cycle of 60 s, the frequency corresponding to the fundamental stimulus is ~0.017 Hz. Each imaging run had a duration of 435 s. Subject head motions were minimized by restricting pads carefully placed within the head coil.

Functional and structural images of the brain were acquired with a 3 T Philips Achieva scanner (Philips Healthcare, Inc., Best, Netherlands) using a 32-channel head coil at the Vanderbilt University Institute of Imaging Science. BOLD-sensitive functional images were obtained using a single shot T_2*-weighted gradient echo (GE), echo planar imaging (EPI) sequence (TR = 3 s, TE = 45 ms, matrix size = 80 × 80, FOV = 240 × 240 mm^2, 43 axial slices each 3 mm thick, and 145 vol). High resolution T_1-weighted images were acquired using a multi-shot, 3D GE sequence ($1 \times 1 \times 1$ mm^3 nominal resolution). Diffusion weighted images (DWI) were acquired using a single-shot, spin echo, EPI sequence (b = 1000 s/mm^2, 32 diffusion-sensitizing directions, TR = 8.5 s, TE = 65 ms, SENSE factor = 3, matrix size = 128 × 128, FOV = 256 × 256, 68 axial slices each 2 mm thick with zero gap).

2.2. Preprocessing of functional and anatomical MRI

Preprocessing of the MRI data was implemented with SPM12 (http://www.fil.ion.ucl.ac.uk/spm), using the embedded functional modules and default parameter settings unless otherwise noted. First, T_2*-weighted images were corrected for slice timing (module *Slice timing*) and head motion (module *Realign*); two subjects with large head motion (>2 mm in translation or >2° in rotation) were excluded from further analyses.[1] Second, T_1-weighted images were segmented (module *Segment*) into WM, GM and cerebrospinal fluid (CSF), and the segmented images were co-registered to the motion-corrected mean T_2*-weighted images (module *Coregister*). Third, the T_2*-weighted images preprocessed above were normalized into the MNI (Montreal Neurological Institute) space (module *Normalise*), along with the co-registered T_1-weighted images and the segmented volumes. Fourth, the T_2*-weighted images (in MNI space) were partitioned into WM and GM volumes using their respective segments. To minimize potential partial volume effects from nearby structures, the WM volume was confined within a tightly thresholded WM segment (>0.9), and spatial smoothing with a 4 mm full-width at half maximum (FWHM) Gaussian kernel was performed separately within the WM and GM volumes of each subject (module *Smooth*). Finally, linear trends in the T_2*-weighted time series were removed from the smoothed

[1] One of the 12 subjects studied had z-translation slightly greater than 2 mm. Temporal and frequency profiles of the head motion parameters, and their impact on detection of white matter activations are presented in Supplementary materials A-C.

images, which were then low-pass filtered (<0.1 Hz) using in-house MATLAB codes. We did not remove the global time series from the time series because global variations may reflect important neural components (Hahamy et al., 2014).

2.3. Analysis of frequency spectra of BOLD signals

Frequency spectra of BOLD signals in response to visual stimulation were calculated and used to locate activated regions in each subject. To begin with, each preprocessed time series in WM was divided by the mean standard deviation of the WM volume for each subject, and were subsequently averaged across the twelve subjects to further improve signal-to-noise ratio (SNR). Frequency spectra of the subject-averaged BOLD signals in the common WM volume in MNI space (defined as the intersection of the twelve individual WM volumes) were then computed voxel-by-voxel using the FFT algorithm in MATLAB, and the magnitude at the frequency corresponding to the fundamental stimulus frequency (~0.017 Hz) was obtained. The map of the magnitude at the stimulus frequency (MSF) was then superimposed onto T_1-weighted images. In the meantime, the MSF map of GM was also obtained using the same procedure as above.

2.4. Reconstruction of fiber pathways related to visual activities from DWI data

Diffusion tensors were computed from the DWI data using a least squares approach (Jones and Cercignani, 2010) with in-house software. A modified probabilistic tracking method (Friman et al., 2006) was employed to reconstruct WM fiber tracts related to visual functions. Fiber tracking started with definitions of seed regions of interest (ROI), which involved the following steps. First, ten fiber bundles (four in each hemisphere and two commissures) were selected from the JHU ICBM-DTI-81 WM atlas and the stereotaxic atlas of fibers (Mori et al., 2008; Bürgel et al., 2006). These bundles included bilateral optic radiation (OR), bilateral fornix (cres) (FXC), splenium of corpus callosum (SCC), pontine crossing (PC), bilateral tapetum (TAP), and bilateral medial lemniscus (ML), which were selected *a priori* as the power of their responses to visual stimulation was found to be greatest (Ding et al., 2018). In addition, bilateral posterior limbs of internal capsules (PLIC) were also included because they contain projection fibers that connect to the parietal eye field (Pierrot-Deseilligny et al., 1995) and were found to have strong power response to visual stimulation in our previous work as well (Ding et al., 2018). Second, skeletons of the above twelve bundles were extracted by a morphological erosion procedure, and these skeletons were used to define the seed ROIs. Finally, the seed ROIs, as well as the original bundles and T_1-weighted images, were transformed to the DWI space by non-linearly co-registering with the non-diffusion weighted (b = 0) image for each subject. The transformation used the SPM12 module *Normalise* with inverse transformation parameters automatically generated by segmenting the T_1-weighted images in the individual DWI space.

With the definitions of the seed ROIs above, probabilistic fiber tracking was implemented for each bundle separately. A voxel within the seed ROI was randomly chosen as the seed point, and the track propagated along a randomly perturbed principal direction of the diffusion tensor until the tracking front exceeded the boundary of the bundle (treated as a successful fiber) or reached any of three other termination criteria (angle between the directions of two successive steps>60°; FA<0.3; tracking steps>10). Note that, because the PC in the JHU atlas was defined much smaller than the true anatomy (Mori et al., 2008), we first expanded it by convolving with a 3 × 3 × 3 kernel and then used the following termination criteria to allow a fuller range of fibers to be tracked: angle between the directions of two successive steps>78.5°; FA<0.1; tracking steps>60. The tracking process was repeated with the number of repetitions equal to 100 times the total number of voxels in the seed ROI, and only successful fibers were retained for further analysis.

The fiber tracking procedure yielded a probability density of fibers (PDF) for each voxel, i.e., the number of fibers traversing the voxel divided by the total number of successful fibers. Finally, the PDF maps were spatially normalized into the MNI space (module *Normalise*) to compare with the MSF maps derived from the BOLD frequency spectra.

2.5. Analysis of sensitivity for detecting white matter activation

We hypothesize that WM activations should coincide with WM tracts so that the degree of concordance of activation maps with fiber density is an indirect metric of sensitivity for reliable detection. To examine the influence of the number of subjects in a group analysis, we repeated the above procedures for subject group sizes of one to twelve. For each group size *n*, the mean MSF in the WM volume was calculated from all possible *n*-combinations of the twelve subjects (i.e., 12, 66, 220, 495, 792, 924, 792, 495, 220, 66, 12, 1 combinations for $n = 1, \ldots, 12$ respectively). The mean MSF maps were then compared with the PDF maps using Dice coefficients (Dice, 1945). In addition, the standard deviation of the Dice coefficient for each group size *n* was computed from the set of individual Dice coefficients between the MSF of each *n*-combination and the PDF maps.

2.6. Analysis of temporal coefficient of variation (CV)

To explore differences in signal characteristics between GM and WM, we performed statistical analyses on BOLD time series in both a resting state and in response to visual stimulation. The stimuli were presented as described earlier in a standard block design. We first calculated the mean signal intensity (SI) and standard deviation (SD) of each subject's BOLD time series, and derived the values of coefficients of variations (CV = the standard deviation divided by the mean). CV here incorporates the variance within the blocks as well as the modulation caused by switching between conditions. Three representative brain regions were chosen for statistical analysis: activated GM and WM regions, and non-activated WM region. The activated GM region was defined as voxels whose MSF was >0.4 maximum MSF (MMSF) within the GM volume, and the activated WM region was defined within the WM volume using the same criterion. The non-activated WM region was defined as voxels in which MSF was <0.2 MMSF within the WM volume. The values of SI, SD and CV of the BOLD time series were compared among the three brain regions for resting state and visual stimulation conditions separately. Two-tailed, paired t-tests were used for all the statistical testing.

3. Results

3.1. Functional activations in white matter under visual stimulation

MSF maps calculated from BOLD signals in WM under visual stimulation are shown in Fig. 1, in which the MSF was thresholded at 0.4 MMSF. Overall, the activated WM voxels tended to form a number of large clusters, with OR well recognizable in the second row of the figure (pointed by yellow arrows). Fig. 1 also includes activated GM voxels, which tended to form clusters in areas corresponding to the primary visual cortex (V1, pointed by the green arrow).

Polarities of the BOLD responses are shown voxel-wise in Fig. 2, in which the yellow contours denote the WM boundaries, and red/blue color represents positive/negative correlations with the mean time series of activated voxels in the V1 respectively. The negative correlations were primarily distributed near the edges of lateral ventricles or other CSF stores or in the middle of WM. Because negative correlations have complex biophysical origins (Bianciardi et al., 2011), which will be discussed in detail later, they were excluded from our subsequent analysis (see Supplementary materials A for polarity maps of individual subjects).

Fig. 3 shows signal waveforms and their corresponding frequency spectra of BOLD signals from activated voxels in the OR, which was defined to be voxels within the OR mask with MSF >0.4 MMSF. The

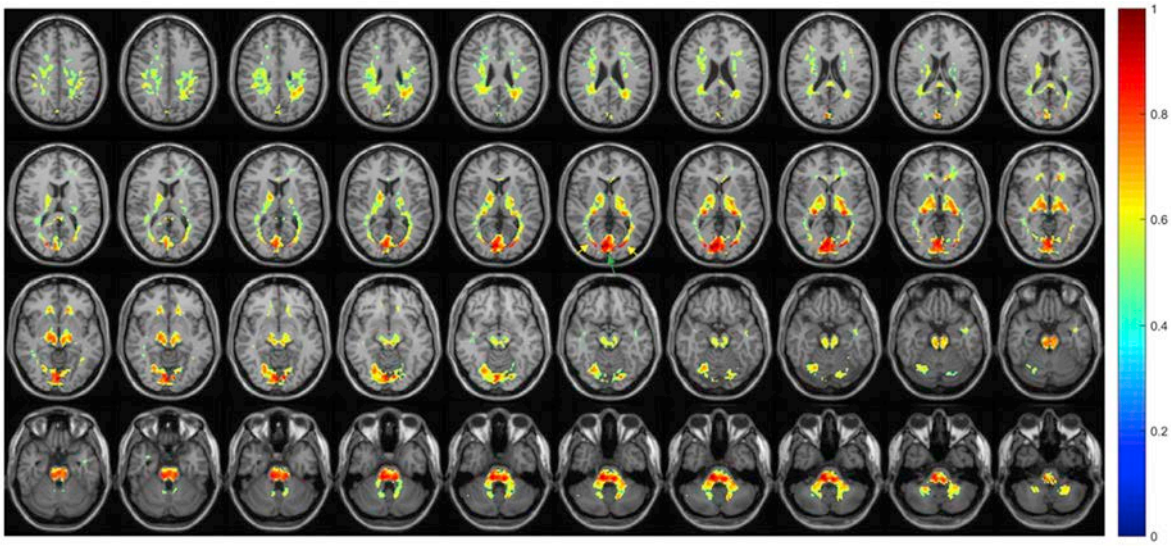

Fig. 1. Distributions of the magnitude at the stimulus frequency in BOLD signals in WM and GM during visual stimulation. The MSF is thresholded at 0.4 MMSF for both WM and GM. Right side of the images is the subject's left. Yellow arrows point to the OR, and the green arrow points to the V1.

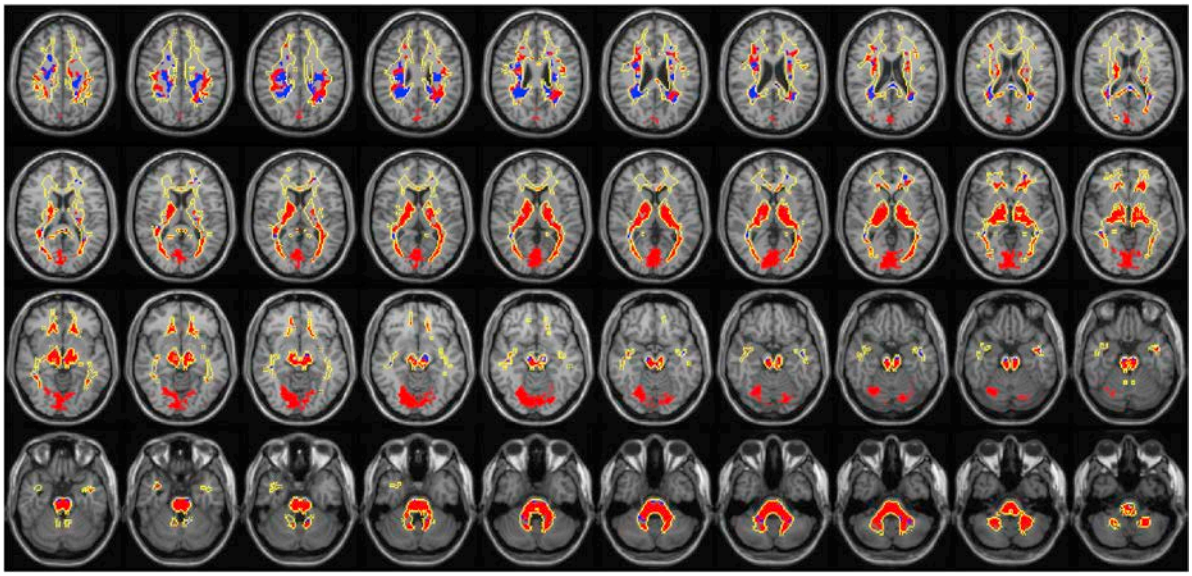

Fig. 2. Polarities of BOLD responses in WM and GM. Red and blue color denotes positive and negative correlation with the mean time series of activated voxels in the V1 respectively. Yellow contours demarcate WM boundaries.

BOLD signals in the OR exhibited clear periodicity and high synchronicity with the stimulus waveforms, as expected. As a comparison, signal waveforms and their frequency spectra of activated voxels in the V1 during visual stimulation are also given in Fig. 3. It can be readily appreciated that variations in the V1 were very similar to those in the OR, both of which exhibited much larger MSF than other frequencies. Stimulus-induced signal increases from the baseline were 1.78% and 5.29% respectively for the OR and V1.

MSF maps from the resting state BOLD signals are shown in Fig. 4. In contrast to the MSF maps from the visual stimulation in Fig. 1, there were only a few small clusters of WM voxels that reached the threshold of 0.4, most of which were presumably due to signal noise. The greatly reduced number of WM voxels with high MSF confirms that the large number of higher values seen in Fig. 1 arise from the effects of visual stimulation.

The MSF maps from voxel-wise detection of WM under visual stimulation in the frequency domain are compared with T-maps in Fig. 5, which were obtained from a second level analysis of the twelve subjects studied using the general linear model in SPM12. It can be seen that, at the t-statistic threshold $T > 1.96$, which corresponds to $p < 0.05$, the distribution of activated WM voxels in the T-maps bears large similarity to the distribution of WM voxels in Fig. 1 (after discounting the negative responses shown in Fig. 2), with a Dice similarity of 0.66 between the two maps. For completeness, the second level analysis in SPM12 was also implemented on GM, with activated voxels superimposed in this figure as well. Note that for fair comparisons, no clusters were removed nor were multiple comparisons corrected. Also of note, these T-maps were computed on the basis of the canonical hemodynamic response function (HRF) for GM; thus it can be anticipated that detection of WM activations could be improved if a WM-specific HRF were used (Courtemanche et al., 2017).

3.2. Reconstruction of anatomical visual pathways by DTI tractography

PDF maps of the visual circuitry obtained from DTI tractography are

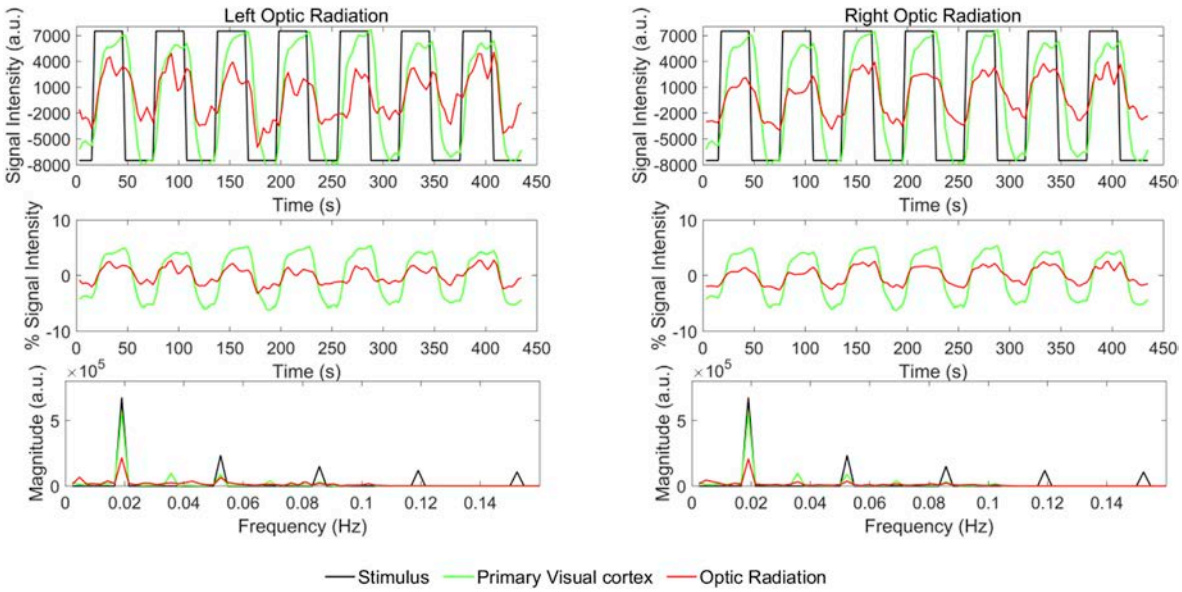

Fig. 3. Signal waveforms and frequency spectra in activated voxels of OR (red) and V1 (green) during visual stimulation. Voxels in the OR and V1 with MSF above 0.4 MMSF were defined as activated voxels. The BOLD time courses in the top row are average intensities of the twelve subjects studied, and the time courses in the middle row are average percent changes in signal intensities. Black curves in the top and bottom rows are the stimuli waveforms and frequency spectra. Stimulus-induced signal increases from resting period were 1.78% and 5.29% for the OR and V1 respectively.

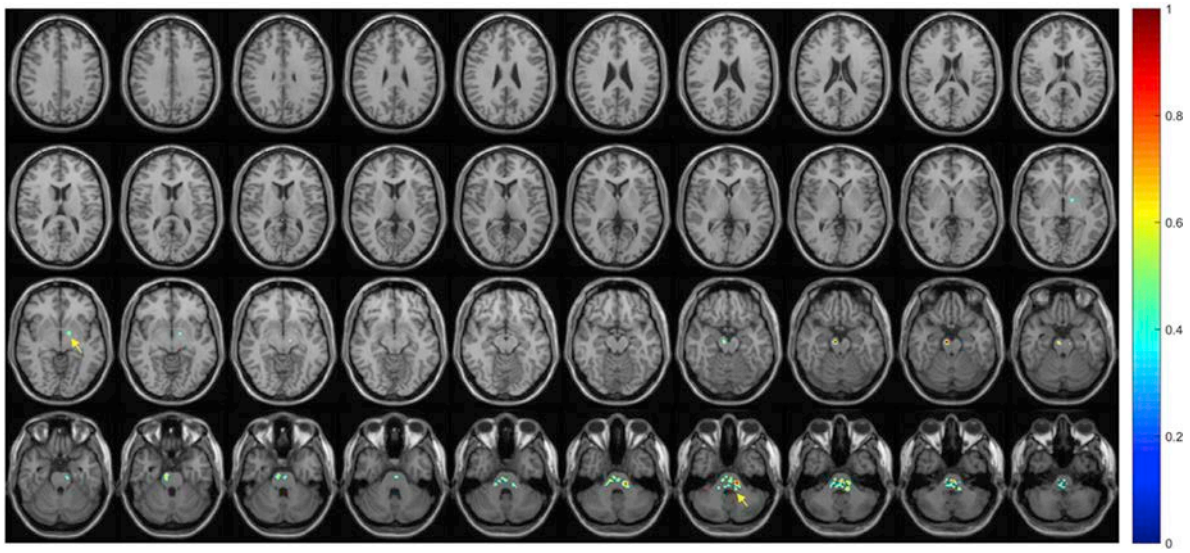

Fig. 4. Distributions of the magnitude corresponding to the frequency of the visual stimulation in a resting state. The threshold level is the same as in the stimulation condition. Right side of the images is the subject's left. Yellow arrows point to supra-threshold clusters.

shown in Fig. 6, where the color represents the PDF averaged across the twelve subjects studied. As can be seen, the PDF maps closely resemble the distribution of WM voxels in Fig. 1. To measure the similarity between the density distributions of the reconstructed visual pathways and the distribution of activated WM voxels, we computed the Dice similarity coefficient between the PDF and MSF maps at different threshold levels (To allow some tolerance on image mismatch, the PDF maps were dilated with an 18-neighborhood 3D kernel prior to the computation). Fig. 7 shows the Dice coefficient had a maximum value of similarity around 0.67 when the thresholds for MSF$>\approx$0.3 and PDF$\approx$0.2.

3.3. Variation of sensitivity in detecting WM activation with group size

The relative sensitivity for detecting WM activation in a group, as ensured by the degree of concordance with fiber density, was evaluated by comparing the Dice coefficients between the PDF and MSF maps for different group sizes, as shown in Fig. 8. It can be seen that Dice coefficient was approximately 0.45 at the level of individual subjects, and increased with the size of the subject group. Note that the Dice similarity coefficient tended to stabilize around 0.65 when the group size reached six, beyond which further increases were quite small. Also of note, the variability in the Dice coefficient was relatively large when the group size was small, and gradually decreased with increases in the group size, as indicated by the standard deviation lines.

3.4. Comparisons of BOLD time series among three representative brain regions

BOLD signal properties in a resting state and under visual stimulation within three representative GM and WM regions are compared in Fig. 9.

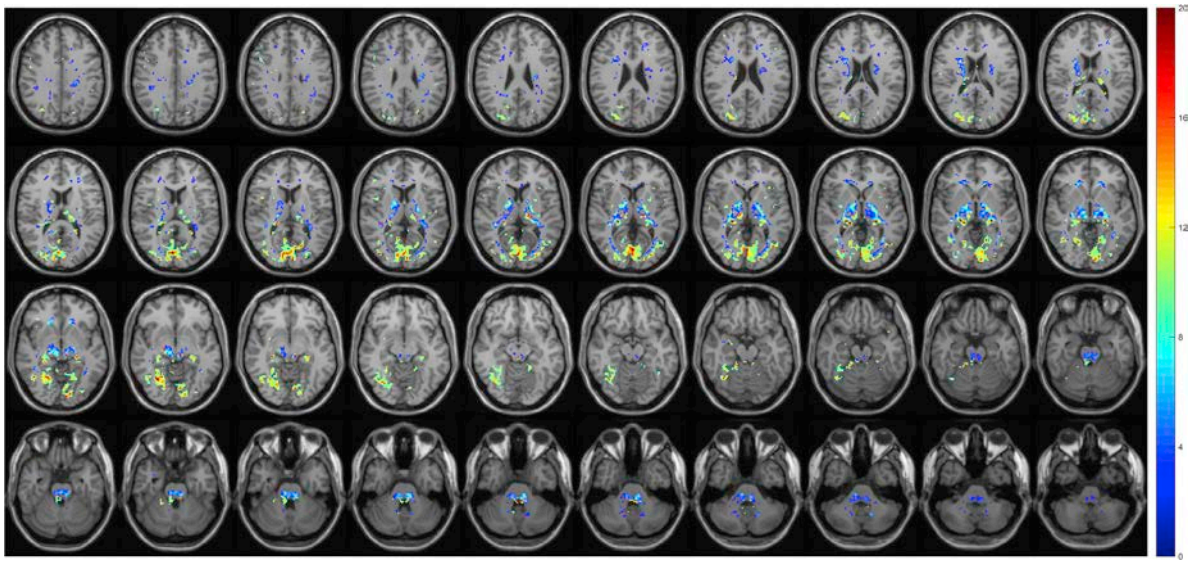

Fig. 5. T-maps of WM and GM signals during visual stimulation. The t-statistic threshold is $T > 1.96$ ($p < 0.05$) for WM and $T > 5$ ($p < 10^{-6}$) for GM. Cluster size threshold is 0 for both WM and GM. No corrections for multiple comparisons were performed.

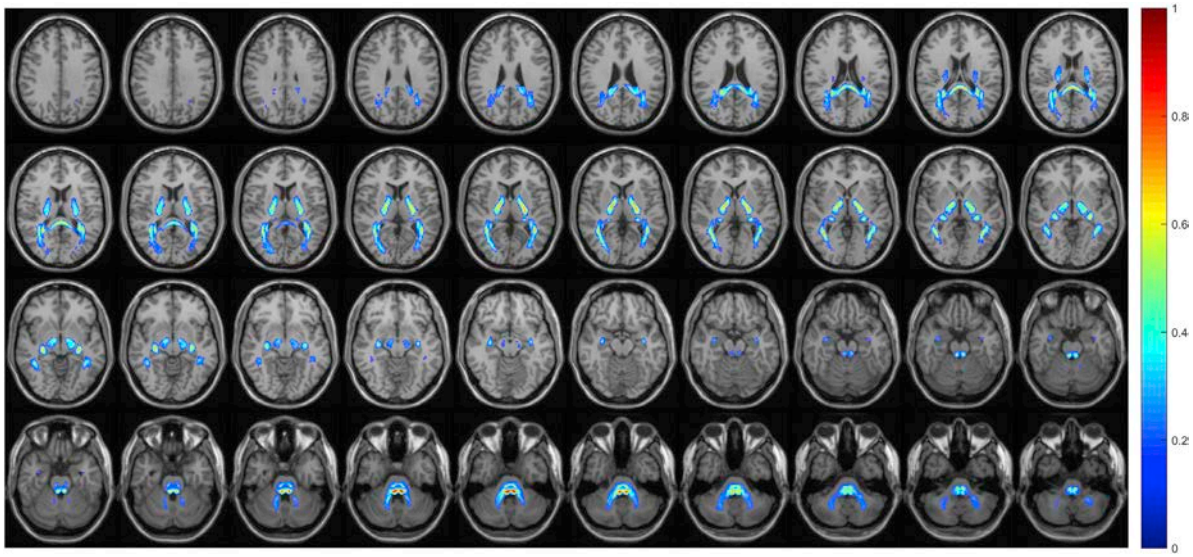

Fig. 6. Distributions of probability density of fibers in the visual system. Twelve WM bundles in each subject were tracked from their skeletons using probabilistic fiber tracking from DTI data. The probability density is the average of the twelve subjects studied.

The mean SI during visual stimulation (including only 3rd-10th TRs in each block of checkerboard flashing) was 6.17% and 4.63% greater than in resting state for activated GM and WM region respectively, and decreased 2.84% from the resting state for non-activated WM region (Fig. 9A). While the mean SI changes were relatively small during visual stimulation for all the three regions, the SD was much greater in the stimulation condition than in a resting state for both the activated GM and WM regions ($p < 0.01$), whereas the difference in SD was not significant within the non-activated WM region (Fig. 9B). Similar differences can also be observed in Fig. 9C.

Quantitative comparisons between the ratios of the CV under visual stimulation and in a resting state show that the ratio for the activated WM region was 2.82, which was ~61% of the ratio for the activated GM region (=4.61). To estimate the contribution of signal fluctuations due to steady state stimulations to the total signal variations, we further computed the CV during the checkerboard flashing period (shown in striped portions of the green bars in Fig. 9C, computed from 3rd-10th TRs after the onset of stimulation) and found that the ratios of the CV to those in the resting state were 1.51 and 1.72 for the activated GM and WM regions respectively,[2] and the ratios to the total CV were 0.33 and 0.61 for the activated GM and WM regions respectively. This indicates that the steady state stimulations enhanced signal fluctuations in activated WM region relatively more than in activated GM region, and they contributed ~60% to the total signal variance in activated WM region.

4. Discussion

In this study we examined the robustness and sensitivity of voxel-wise detection of WM activations under visual stimulations. By analyzing the spatial distributions of BOLD signal frequency spectra, we have

[2] $P = 0.0036$ for activated GM region and $p = 0.0200$ for activated WM region from paired, two-tailed t-tests of the differences in CV between resting and steady states.

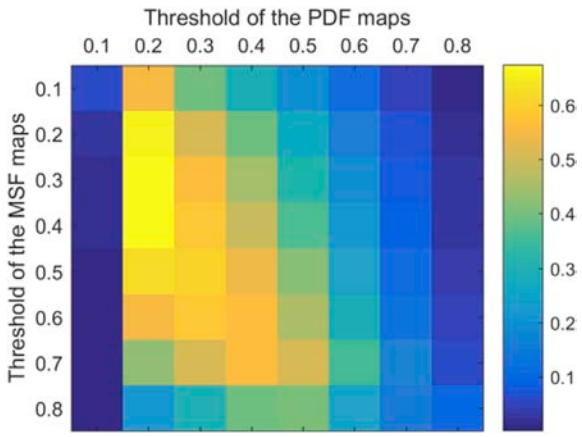

Fig. 7. Dice similarity coefficient between the MSF and PDF maps with different combinations of threshold levels.

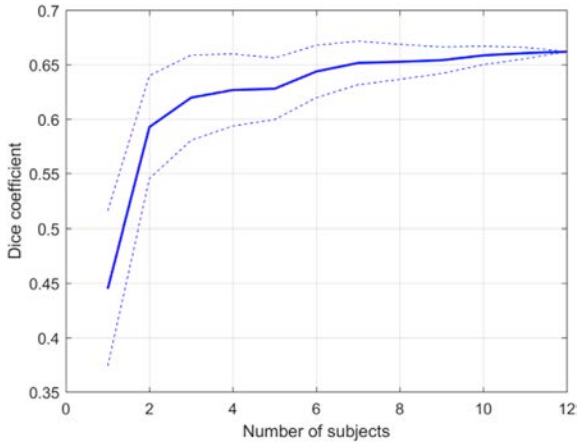

Fig. 8. Variations of Dice coefficient with the group size. The abscissa is the size of the subject group, and the ordinate is Dice coefficient between the average MSF map and the PDF maps. For each group size *n*, the average MSF map was calculated from all possible *n*-combinations from the set of twelve subjects studied. Dotted lines are the corresponding standard deviation, which were computed from the set of individual Dice coefficients between the MSF of each *n*-combination and the PDF maps.

demonstrated that WM voxels were activated mostly along the fiber pathways relevant to visual activity. The locations of activated WM voxels were grossly consistent with maps reconstructed by DTI fiber tracking. Our further analysis showed that the degree of agreement between positively identified WM activations and diffusion fiber density was proportional to the size of the study group but tended to stabilize after a certain point. Comparisons of BOLD signals between resting state and visual stimulation conditions revealed that the coefficient of variation in WM during a period of stimulation was significantly increased by visual stimulations, and that contributions of steady state fluctuations were much greater than "switching effects" between visual stimulation and rest to the signal variance in activated WM regions.

4.1. Visual circuits

The voxels showing visual activation in WM lay primarily within the OR, SCC, TAP, FXC, ML, PC and PLIC bundles. The OR carries neural signals from the lateral geniculate body to the visual cortex (Kitajima et al., 1996). The SCC contributes to the integration of visual information (Fabri and Polonara, 2013), and the FXC has been implicated in visual memory functions (Miller et al., 2015). It has been reported that WM fibers connect SCC with the occipital cortex via the forceps major and the TAP (Caspers et al., 2015). The ML carries axons from the face and eyes via the trigeminal nerve synapse to the thalamus (Zwergal et al., 2008). The pontine cells receive inputs from the visual cortex or the superior colliculus and have extensive projections onto the cerebellar cortex (Glickstein, 2000). The PLIC contains fibers associated with saccadic eye movements (Gaymard et al., 2003).

4.2. BOLD signal profiles

Based on statistical comparisons of BOLD time series between resting state and visual stimulation as well as among three different brain regions, a number of observations are particularly noteworthy. First, the mean signal intensities of the BOLD time series have small differences between resting state and visual stimulation, but the standard deviation is considerably greater under visual stimulation. Second, the CV of BOLD signals, which characterizes the extent of fluctuations in each time series, is greater during visual stimulation than in a resting state; the CV in activated GM is greater than in activated WM voxels, both of which are greater than that in non-activated WM voxels. The greater CV in activated GM region may partly explain the greater detectability of GM activations by conventional means than WM activations in which both total CV and contributions of "switching effects" are much smaller, though the increase in fluctuations during each block reduces the overall sensitivity to switching effects. Third, the sensitivity of WM signal detection using our criterion (which quantifies the number of WM fibers that appear to activate) increases with the number of studies averaged within the subject group, and our experiments confirmed that the sensitivity tends to stabilize when the group size increases. Obviously, the gain in

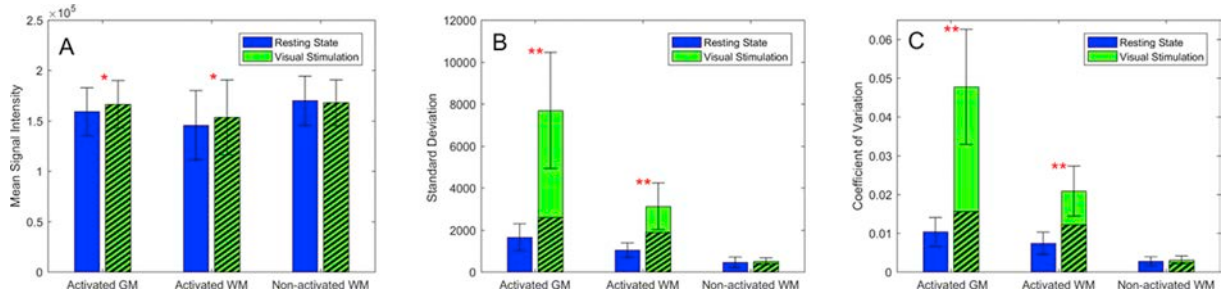

Fig. 9. Comparisons of BOLD signal profiles among three representative brain regions. (A) Mean signal intensity, (B) Standard deviation, and (C) Coefficient of variations in BOLD time series. From left to right in panels (A–C) are activated GM region, activated and non-activated WM regions. Blue and green bars denote resting state and visual stimulation respectively; error bars denote standard deviations of the measurements; asterisks (*) and (**) denote $p < 0.05$ and $p < 0.01$ from paired, two tailed t-tests respectively. Stripes in the green bars denote the portions measured from 3rd–10th TRs after the onset of stimulation. The number of voxels for computing statistics of the activated GM, WM and non-activated WM regions are respectively 3980 (all activated voxels), 1430 (all activated voxels) and 1460 (down sampled).

sensitivity from signal averaging is attributable to increased SNR, and similar increases would be anticipated by averaging a larger number of trials for each subject.

Polarities of BOLD response: In this work, we have observed both positive and negative BOLD correlations in WM with the primary visual cortex. The negative correlations are distributed mostly near the edges of CSF stores or in the middle of WM, similar to the findings in previous studies (Bianciardi et al., 2011; Bright et al., 2014). Mechanistically, the negativity in BOLD responses may be caused by neuronal inhibition (Shmuel et al., 2006) or vascular stealing (Harel et al., 2002), or interpreted by blood volume effects in large veins downstream to the activation site with the nature of pure anti-phasing rather than delayed hemodynamic response (Bianciardi et al., 2011). We should note that, although a long time delay of ~20 s in WM (relative to GM) during hypercapnia challenges has been observed (Thomas et al., 2014), which is presumably attributable to long buildup time required for extravascular CO_2 in WM, the time delay in WM induced by neural events has been found typically within a few seconds (Yarkoni et al., 2009; Courtemanche et al., 2017). Thus, given the stimulation cycle of one minute in this study, it can be inferred that the negative correlations we observed were due to anti-phasing resulting from draining vein effects or other mechanisms instead of local hemodynamic delay.

Recognizing the complex origins of negative correlations, we excluded them from further analysis so that focus was given to detections of only positively correlated voxels to minimize potential false positives. The positive correlations, in principle, might arise from vein draining effects as well, as previously found in the cortex (Turner, 2002). From the architecture of the brain venous systems, however, the possibility that deoxygenated blood is drained from cortical GM to deep WM is rather small. In fact, there are two venous systems in normal neuroanatomy: a superficial venous system that drains deoxygenated blood in the cortex and superficial WM into dural venous sinuses via cortical veins, and a deep venous system that drains deoxygenated blood in deep WM into subependymal veins (Ru\'z and HaGailloud, 2009). Presumably the spatially non-overlapping nature of the brain venous architecture has evolutionary advantages in terms of cost-efficiency, space economics in brain parenchyma, and perhaps the dissipation efficiency of heat from metabolism. Anomalous draining from cortical GM into the deep venous system via WM does exist, but the incidence rate of such anomalous draining route is below 3% (Ru\'z and HaGailloud, 2009). Thus it is highly unlikely that the positive correlations we observed were driven by venous draining effects from "upstream" GM activities in the cortex.

4.3. Limitations

It should be pointed out that this study comes with some technical limitations. Most notably, the method we used for detecting BOLD effects relies on isolating frequency components of MRI signals in response to stimuli with a well defined, known frequency. This approach would not be applicable to other experimental designs. However, more conventional linear model approaches should also be suitable as long as the HRF selected is appropriate for WM and takes account of potential regional differences. Also, our analysis was based on signal averaging across a small group of twelve subjects for the purpose of increasing SNR, but higher SNR in individuals could be achieved by, for example, acquiring longer runs (assuming physiological noise averages over time) or using lower resolution, higher field strength or alternative acquisition sequences. Moreover, the spatial resolutions of BOLD and DWI data are different in this study, which inevitably creates matching errors and hence affects the accuracy of comparisons between the findings from the two modalities. The fiber bundles reconstructed by DTI tractography may contain fibers that are irrelevant to visual activity, which could account for the measured Dice coefficients of our comparisons.

In this study, we have observed high variability in white matter activations (both in the extent and location) across individual subjects. There are potentially many confounds that might have contributed to this variability, which include inter-subject variability in vascular distributions and sensitivity of visual circuitry to stimuli, variable levels of attention during the experiment, or differences in field inhomogeneity profiles among the individuals. To add to the complications, because white matter has much reduced vascular density (Nonaka et al., 2003), which translates to proportionally decreased BOLD signals therein, the effects of these confounds, as well as from other origins, tend to be greatly magnified.

It should be mentioned that a major concern in detection of WM activations with fMRI is whether the detected signals are due to partial volume effects from adjacent GM. In this study, these are meticulously avoided by tightly thresholding the WM and confining all subsequent processing and analysis within the WM volume. Another common concern is that the relatively weaker hemodynamic response in WM is more susceptible to random noise, so that the detected activation may be false positive artifacts. Potential effects from random noise are largely alleviated in this study by spatially smoothing BOLD signals within the WM volume and then averaging them across the group of subjects under study.

Finally we emphasize that, although this study demonstrates the feasibility of detecting WM activations on the basis of stimulus frequency, other approaches conventionally used in the field of electroencephalography may also be employed for this purpose, such as examining the spectral coherence between the stimulus and response signals (Wada et al., 1998). However, while methods based on the spectral coherence possess the advantage of including other signal harmonics (in addition to the fundamental) so that the power of detection could be greater, they also suffer from the confounding effects of background signals, which efforts have been made to suppress (Miranda de Sá et al., 2001). The pros and cons of our method and those based on spectral coherences will be examined in our future work.

In summary, to explore the detectability of functional activation in WM with fMRI, we studied BOLD time series in both the frequency and temporal domains. There are three major findings from this work. First, analysis of frequency in BOLD time series allows activated WM regions to be detected voxel-wise. It was demonstrated that, compared to resting state, functional activations in response to visual stimulation exist along fiber pathways related to visual activities, and that the patterns of activation are consistent with fiber tracts reconstructed by using DTI. Second, the sensitivity of detecting WM activations increases with the size of the study group. Third, there is only a small difference in mean signal intensity of BOLD time series of WM between resting state and visual stimulation conditions, but the signal standard deviation (and also coefficient of variations) is considerably greater during visual stimulation. Taken together these findings are consistent with the premise that BOLD signals in WM reflect neural activities that can be detected by appropriate methods, and they offer the potential of depicting complete functional networks in the human brain that encompass both GM regions and WM pathways, which is one of our major directions in the future.

Acknowledgments

This work is supported by NIH grants R01 NS093669 (JCG), R01 HD044073 (LEC), R01 HD067254 (LEC), U54 HD083211 (LEC), F31 HD090923 (SKB), QN2016169 (YH, Youth Foundation of Hebei Province Department of Education, China), and CSC201408130196 (YH, China Scholarship Council).

Appendix A. Supplementary data

Supplementary data related to this article can be found at https://doi.org/10.1016/j.neuroimage.2018.08.049.

References

Azevedo, F.A., et al., 2009. Equal numbers of neuronal and nonneuronal cells make the human brain an isometrically scaled-up primate brain. J. Comp. Neurol. 513, 532–541.

Bianciardi, M., Fukunaga, M., Van Gelderen, P., De Zwart, J.A., Duyn, J.H., 2011. Negative BOLD-fMRI signals in large cerebral veins. J. Cerebr. Blood Flow Metabol. 31, 401–412.

Biswal, B., Zerrin Yetkin, F., Haughton, V.M., Hyde, J.S., 1995. Functional connectivity in the motor cortex of resting human brain using echo-planar mri. Magn. Reson. Med. 34, 537–541.

Bright, M.G., Bianciardi, M., de Zwart, J.A., Murphy, K., Duyn, J.H., 2014. Early anti-correlated BOLD signal changes of physiologic origin. Neuroimage 87, 287–296.

Buckner, R.L., Andrews-Hanna, J.R., Schacter, D.L., 2008. The brain's default network. Ann. N. Y. Acad. Sci. 1124, 1–38.

Bürgel, U., et al., 2006. White matter fiber tracts of the human brain: three-dimensional mapping at microscopic resolution, topography and intersubject variability. Neuroimage 29, 1092–1105.

Caspers, S., et al., 2015. Target sites for transcallosal fibers in human visual cortex-a combined diffusion and polarized light imaging study. Cortex 72, 40–53.

Courtemanche, M.J., Sparrey, C.J., Song, X., MacKay, A., D'Arcy, R.C., 2017. Detecting white matter activity using conventional 3 Tesla fMRI: an evaluation of standard field strength and hemodynamic response function. Neuroimage 169, 145–150.

Dice, L.R., 1945. Measures of the amount of ecologic association between species. Ecology 26, 297–302.

Ding, Z., et al., 2013. Spatio-temporal correlation tensors reveal functional structure in human brain. PLoS One 8, e82107.

Ding, Z., et al., 2016. Visualizing functional pathways in the human brain using correlation tensors and magnetic resonance imaging. Magn. Reson. Imaging 34, 8–17.

Ding, Z., et al., 2018. Detection of synchronous brain activity in white matter tracts at rest and under functional loading. Proc. Natl. Acad. Sci. Unit. States Am. 115, 595–600.

Fabri, M., Polonara, G., 2013. Functional topography of human corpus callosum: an FMRI mapping study. Neural Plast. 2013.

Fabri, M., Polonara, G., Mascioli, G., Salvolini, U., Manzoni, T., 2011. Topographical organization of human corpus callosum: an fMRI mapping study. Brain Res. 1370, 99–111.

Fox, M.D., Raichle, M.E., 2007. Spontaneous fluctuations in brain activity observed with functional magnetic resonance imaging. Nat. Rev. Neurosci. 8, 700–711.

Fraser, L.M., Stevens, M.T., D'Arcy, R.C., Beyea, S.D., 2012. White versus gray matter: fMRI hemodynamic responses show similar characteristics, but differ in peak amplitude. BMC Neurosci. 13, 91.

Friman, O., Farneback, G., Westin, C.-F., 2006. A Bayesian approach for stochastic white matter tractography. IEEE Trans. Med. Imag. 25, 965–978.

Gawryluk, J.R., Brewer, K.D., Beyea, S.D., D'arcy, R.C., 2009. Optimizing the detection of white matter fMRI using asymmetric spin echo spiral. Neuroimage 45, 83–88.

Gawryluk, J.R., Mazerolle, E.L., D'Arcy, R.C., 2014. Does functional MRI detect activation in white matter? A review of emerging evidence, issues, and future directions. Front. Neurosci. 8, 239.

Gaymard, B., Lynch, J., Ploner, C., Condy, C., Rivaud-Pechoux, S., 2003. The parieto-collicular pathway: anatomical location and contribution to saccade generation. Eur. J. Neurosci. 17, 1518–1526.

Glickstein, M., 2000. How are visual areas of the brain connected to motor areas for the sensory guidance of movement? Trends Neurosci. 23, 613–617.

Glover, G.H., 2011. Overview of functional magnetic resonance imaging. Neurosurgery Clinics 22, 133–139.

Gore, J.C., 2003. Principles and practice of functional MRI of the human brain. J. Clin. Invest. 112, 4–9.

Hahamy, A., et al., 2014. Save the global: global signal connectivity as a tool for studying clinical populations with functional magnetic resonance imaging. Brain Connect. 4, 395–403.

Harel, N., Lee, S.-P., Nagaoka, T., Kim, D.-S., Kim, S.-G., 2002. Origin of negative blood oxygenation level—dependent fMRI signals. J. Cerebr. Blood Flow Metabol. 22, 908–917.

Jones, D.K., Cercignani, M., 2010. Twenty-five pitfalls in the analysis of diffusion MRI data. NMR Biomed. 23, 803–820.

Kitajima, M., Korogi, Y., Takahashi, M., Eto, K., 1996. MR signal intensity of the optic radiation. Am. J. Neuroradiol. 17, 1379–1383.

Logothetis, N.K., Wandell, B.A., 2004. Interpreting the BOLD signal. Annu. Rev. Physiol. 66, 735–769.

Marussich, L., Lu, K.H., Wen, H., Liu, Z., 2017. Mapping white-matter functional organization at rest and during naturalistic visual perception. Neuroimage 146, 1128–1141.

Mazerolle, E.L., et al., 2013. Sensitivity to white matter fMRI activation Increases with field strength. PLoS One 8, e58130.

Miller, J.P., et al., 2015. Visual-spatial memory may be enhanced with theta burst deep brain stimulation of the fornix: a preliminary investigation with four cases. Brain 138, 1833–1842.

Miranda de Sá, A.M.F.L., Infantosi, A.F.C., Simpson, D.M., 2001. A statistical technique for measuring synchronism between cortical regions in the EEG during rhythmic stimulation. IEEE Trans. Biomed. Eng. 48, 1211–1215.

Mori, S., et al., 2008. Stereotaxic white matter atlas based on diffusion tensor imaging in an ICBM template. Neuroimage 40, 570–582.

Nonaka, H., et al., 2003. Microvasculature of the human cerebral white matter: arteries of the deep white matter. Neuropathology 23, 111–118.

Ogawa, S., Lee, T.M., Kay, A.R., Tank, D.W., 1990. Brain magnetic resonance imaging with contrast dependent on blood oxygenation. Proc. Natl. Acad. Sci. U.S.A. 87, 9868–9872.

Peer, M., Nitzan, M., Bick, A.S., Levin, N., Arzy, S., 2017. Evidence for functional networks within the human brain's white matter. J. Neurosci. 37, 6394–6407.

Pierrot-Deseilligny, C., Rivaud, S., Gaymard, B., Müri, R., Vermersch, A.I., 1995. Cortical control of saccades. Ann. Neurol. 37, 557–567.

Raichle, M.E., et al., 2001. A default mode of brain function. Proc. Natl. Acad. Sci. U.S.A. 98, 676–682.

Rostrup, E., et al., 2000. Regional differences in the CBF and BOLD responses to hypercapnia: a combined PET and fMRI study. Neuroimage 11, 87–97.

Ruíz, D., Ha, Yilmaz, Gailloud, P., 2009. Cerebral developmental venous anomalies: current concepts. Ann. Neurol. 66, 271–283.

Shmuel, A., Augath, M., Oeltermann, A., Logothetis, N.K., 2006. Negative functional MRI response correlates with decreases in neuronal activity in monkey visual area V1. Nat. Neurosci. 9, 569.

Thomas, B.P., Liu, P., Park, D.C., Van Osch, M.J., Lu, H., 2014. Cerebrovascular reactivity in the brain white matter: magnitude, temporal characteristics, and age effects. J. Cerebr. Blood Flow Metabol. 34, 242–247.

Turner, R., 2002. How much cortex can a vein drain? Downstream dilution of activation-related cerebral blood oxygenation changes. Neuroimage 16, 1062–1067.

Wada, Y., Nanbu, Y., Kikuchi, M., Koshino, Y., Hashimoto, T., 1998. Aberrant functional organization in schizophrenia: analysis of EEG coherence during rest and photic stimulation in drug-naive patients. Neuropsychobiology 38, 63–69.

Wu, X., et al., 2017. Functional connectivity and activity of white matter in somatosensory pathways under tactile stimulations. Neuroimage 152, 371–380.

Yarkoni, T., Barch, D.M., Gray, J.R., Conturo, T.E., Braver, T.S., 2009. BOLD correlates of trial-by-trial reaction time variability in gray and white matter: a multi-study fMRI analysis. PLoS One 4, e4257.

Zwergal, A., Büttner-Ennever, J., Brandt, T., Strupp, M., 2008. An ipsilateral vestibulothalamic tract adjacent to the medial lemniscus in humans. Brain 131, 2928–2935.